Available online at www.sciencedirect.com
ScienceDirect
Journal of the European Ceramic Society 27 (2007) 3311–3316
www.elsevier.com/locate/jeurceramsoc

Nanoindentation on hybrid organic/inorganic silica aerogels

N. de la Rosa-Fox [a,*], V. Morales-Flórez [a], J.A. Toledo-Fernández [a], M. Piñero [b], R. Mendoza-Serna [a], L. Esquivias [c]

[a] *Departamento de Física de la Materia Condensada, Facultad de Ciencias, 11510 Puerto Real, Spain*
[b] *Departamento de Física Aplicada, CASEM, Universidad de Cádiz, Avda/República Saharaui, s/n, 11510 Puerto Real, Cádiz, Spain*
[c] *Departamento de Física de la Materia Condensada, Facultad de Física, Universidad de Sevilla, Spain*

Available online 24 April 2007

Abstract

The hybrid organic/inorganic silica aerogels experiment a drastic mechanical change into rubber behaviour in relation with the pure inorganic silica aerogel as a brittle material. Aerogels were prepared by sol–gel process and drying by venting off the supercritical ethanol, no degradation of the organic polymer was detected. TEOS (tetraethoxysiloxane) and PDMS (polydimethylsiloxane) were used as inorganic and organic precursors, respectively. Depth sensing nanoindentator was used to study the mechanical properties, which is extremely sensitive to small loads (1 mN) and penetration depths (10 nm). The TEOS inorganic clusters and the polymer crosslinking degree influence the microstructure of the hybrid aerogels. Surface indentations maps reveal the different heterogeneities such as the tough silica matrix, the softness of the elastic polymer chains and the plastic microcracks in pores. The values obtained are compatible with the macroscopic ones resulting from uniaxial compression. Creep tests confirm that the compliance parameter increases with the polymer content and results can be theoretically modeled by the Burger model.

Keywords: Sol–gel processes; Creep; Nanoindentation

1. Introduction

Nanoindentation permits to probe the mechanics of nanomaterials[1] and permits direct physical property measurements of heterogeneous materials with high spatial resolution. This technique traditionally has been used to characterize elasto-plastic hard materials; moreover many groups have used this technique on soft tissues, such as demineralized dentin[2] and vascular tissues.[3] The problem of the analytical techniques comes from the influence of interfacial adhesive forces, which can affect the indentation contact area and has not been validated for very soft materials, elastic modulus below 5 MPa. Some authors have demonstrated the validity of the nanoindentation in measuring the elastic modulus of pure PDMS with different degrees of crosslinking.[4]

On the other hand, several studies are concentrated on the sol–gel method and specifically in aerogels.[5] This fact seems to be very useful for the study of such complex structures as the hybrid organic/inorganic aerogels, which are composed by an inorganic phase covalently bonded to an organic polymer chain.

In the present work, the aerogels are prepared with ultrasonic treatment in the liquid state before gelation giving a "*sono-aerogel*".[6] This process known as cavitation, yields to a denser and a finer distribution in the nanostructured solid. When a liquid is exposed to ultrasonic waves creates bubble to growth. Sound waves stress these bubbles, causing them to grow, contract and eventually to implode. With implosion, immense heat and pressure are produced that speed reactions. Every imploding bubble is a microreactor in itself, accelerating reactions unheard of in traditional chemistry. This is due to the extreme heat released upon implosion that creates a local hot spot. The acoustic cavitation bubbles via hot spot formation seem to be responsible of the homogeneous and small size of the silica clusters distribution in these hybrid aerogels.

From a macroscopic mechanical point of view these hybrid aerogels tune from brittle solids to rubber elastomers with the polymer content. As the polymer interlinks the aerogel silica clusters become as elastic solid those provoke the softness of the material, in this way the hardness and the elastic modulus

* Corresponding author. Tel.: +34 956016322; fax: +34 956016288.
E-mail address: nicolas.rosafox@uca.es (N. de la Rosa-Fox).

0955-2219/$ – see front matter © 2007 Elsevier Ltd. All rights reserved.
doi:10.1016/j.jeurceramsoc.2007.02.209

decrease. For that reason, these hybrid aerogels present viscoelasticity from the time dependence of the stress at fixed strain (relaxation) and of the strain at fixed stress (creep).[7]

In order to study more deeply the mechanical properties of organic–inorganic aerogels we have performed creep tests on hybrid aerogels. These essays have been widely used on different kinds of materials, and more precisely on polymers.[8] In this work, we have compared the results obtained from the pure silica aerogel to the maximum permitted polymer content, in order to study the effect of each phase and their interaction during creep. Generally speaking, creep curves show an instantaneous elastic deformation followed by a transitory state of retarded deformation known as primary creep. During this period, it can be understood that the material is suffering a reinforcement process by deformation.[9] Then, the system arrives to the secondary creep, a steady state where the equilibrium is found within the different mechanisms of strain and recovery.

From a rheological point of view, several models can be used for understanding the mechanical behaviour of the studied structure.[10,11] Typically used are the Maxwell model, the Kelvin–Voigt model and the so-called Burger model,[12] a Kelvin chain with only a Voigt element. The Burger model supposes the existence of an immediate pure elastic deformation, a transitory state of retarded elastic deformation and a steady state of viscous flow. For polymeric systems, the Maxwell model[13] as well as the Kelvin–Voigt[18] and the Burger model for the hybrid organic–inorganic composites[14] have been applied previously.

One of the main goals of the current study is to check the validity of the nanoindentation on these hybrid organic/inorganic aerogels.

2. Experimental

2.1. Sample preparation

Silica gels were synthesized by the classical sol–gel method by means of a two-step procedure. First TEOS (tetraethoxysiloxane), as inorganic phase, is partially hydrolyzed understoichiometrically with acid water (pH ∼1) in a molar ratio of TEOS:H_2O of 1:0.84. At this step the solution received an ultrasonic energy of 320 J cm^{-3} resulting a transparent and homogeneous solution. In the second step PDMS (polydimethylsiloxane), as organic phase, is added to complete the hydrolysis reaction with a molar ratio TEOS:H_2O of 1:3.16 with an application of 320 J cm^{-3} ultrasound energy. Several PDMS content were used as the weight percent of the total silica content in the sample. Also was used as organic phase the MTES (methyltriethoxysiloxane). The liquid sol is kept in hermetically close container up to gelification take place. The gel is immersed in extra volume of ethanol for the aging process and to expel the residual water from the pores.

After 1 week of aging the gel is immersed in excess of ethanol to remove the traces of water. At this point the gel is placed in an autoclave and the pore liquor is venting-off above the supercritical conditions of ethanol (240 °C, 63 bar). The supercritical state is attained by slow heating (1 °C/min) in order to minimize the ethanol thermal expansion coefficient, much greater than that of the wet silica gel network. Then the heating produces the evaporation of the additional volume of ethanol that permits to reach the supercritical pressure and temperature (255 °C, 85 bar), in such a way that never cross the vapor–liquid equilibrium curve avoiding capillary pressures on the adjacent pore, then the structure not collapses and the aerogel retains its original shape. In the light of the mechanical test samples were made as cylinders 18 mm long and 8 mm diameter approximately. Density was calculated by weighing the sample with a well-defined geometry.

Sample code will be PDMSX, where X indicates the weight percent of organic polymer in relation with the total silica.

2.2. Nanoindentation

Nanoindentation was measured with a Nanotest automatic device from MicroMaterials Ltd. (UK). It is equipped with a diamond indenter with Berkovich pyramidal tip (100 nm diameter). Load–depth curves were recorded in 25 indentations in line at 20 μm distance, using maximum loads up to 4 mN and load rates ranging 5–75 μN/s. Maps were registered on 10 × 10 grid indentations with 10 μm apart each one, surface was polished at optical level. Creep tests were performed on two kinds of samples: pure silica aerogel and hybrid organic/inorganic aerogel with 50 wt.% of PDMS. Creep data were collected along 3600 s, in a cabinet with controlled humidity around 40% and temperature of 28 °C. The tests were run under different loads in the range from 0.5 to 1.5 mN.

2.3. Mechanical parameters

The initial slope on the unloading branch (stiffness, S) is related to the reduced elastic modulus (E_r) by the following relationship:

$$S = \left(\frac{dP}{dh}\right)_{max} = \frac{2}{\sqrt{\pi}} E_r \sqrt{A}$$

where A is the area of the imprint on the sample, in this case a Berkovich pyramidal tip ($A = 24.5h^2$, h being the depth). The slope S is calculated after least square fitting by the power law proposed function by Oliver and Pharr[15,16] by the form:

$$P = \alpha h^m$$

where α contains geometric constants, both sample and indenter elastic modulus and Poisson's ratio, and m is the power law exponent related with the geometry of the indenter, for a cone $m = 2$. The hardness is calculated simply by $H = P/A$ and the elastic recovery parameter as ERP = $(h_{max} - h_f)/h_{max}$, where h_f is the non-recovered depth of the indenter inside the aerogel sample.

To analyse the creep test, different strategies can be found in the literature. One of the most used techniques is to study the strain rate[17,18,19] $d\varepsilon/dt$. This parameter can be related to some structural parameters[17] and its relationship with the applied

stress σ can be generally written as follows:

$$\dot{\varepsilon} = A\sigma^n \, e^{-(Q/kT)}$$

where A depends on the structure and Q is called the activation energy. The exponent 'n' talks about the different mechanisms that can appear as response of the material to the stress.[18]

On the other hand, the creep compliance can be also studied. It shows how the material acts under a constant load, and it can be defined as

$$J(t) = \frac{\varepsilon(t)}{\sigma_0}$$

Being impossible to define the classical strain in nanoindentation experiments, in the literature the expression for this purpose can be found.[20,21] For a Berkovich tip, the indenter is considered as cone-shaped of semi-apical effective angle $\theta = 71.1°$, bearing in mind that this fact implies an error lower than 3%. Then, the creep compliance can be expressed as follows:

$$J(t) = \frac{A(t)tg\theta}{P_0}$$

where $A(t)$ is the depth-dependent contact area for the Berkovich tip and P_0 is the applied load.

3. Results and discussion

Fig. 1 shows a typical depth–load hysteresis curve, it is apparent the drastic change between both samples, as a first indication the load necessary to provoke a displacement of 1 μm is a 33% greater for the pure silica sample against the hybrid aerogel with a 10 wt.% of polymer content. In this way the polymer chains influence mainly on the stiffness of the silica producing a decrease in the hardness from 226 MPa for the pure silica to 24 MPa for the hybrid aerogel sample, and consequently a better elastic recovery indicated by a bigger depth interval (h_f, h_{max}).

The grid maps results demonstrate the selective sites of the nanoindentation, in all of the cases the load–depth curves are obtained as a fan from a stiffest site (low depth with maximum load) to a softest ones (maximum depth with minimum load),

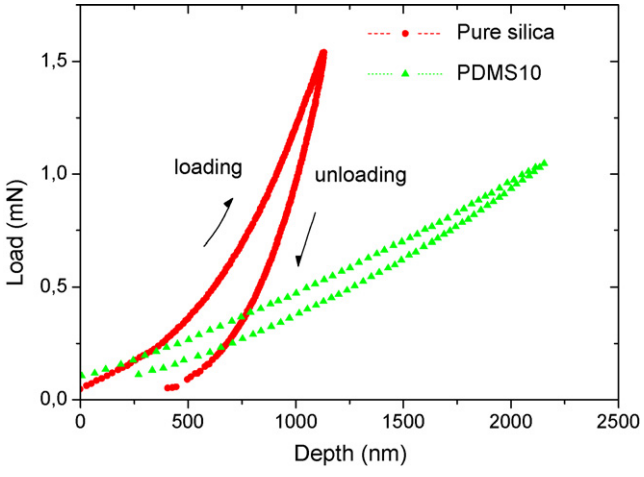

Fig. 1. Depth–load hysteresis curves for the outlined samples. Maximum load at 1.5 mN with a penetration rate of 5 μN/s.

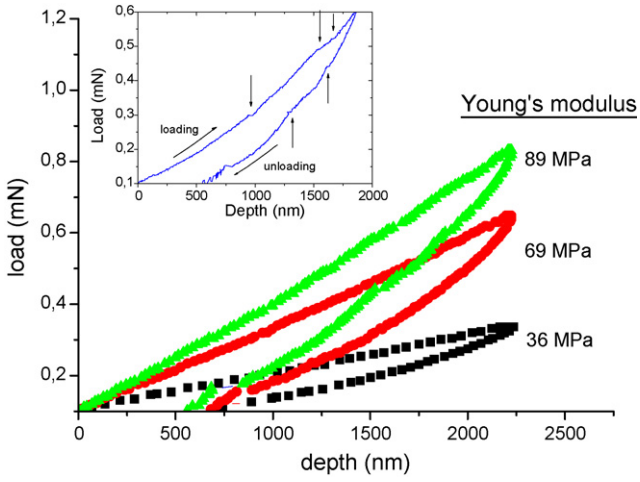

Fig. 2. Three curves for PDMS50 hybrid aerogel at a maximum load of 0.75 mN and 5 μN/s load rate. (Inset) Pop-in and pop-out events indicated with arrows.

three of such sites are shown in Fig. 2, for 50 wt.% polymer content hybrid aerogel. As can be seen the polymer tune the elastic modulus at the different sites, 89, 69 and 36 MPa, respectively, we argued that stiffness sites are dominated by the hard inorganic silica clusters components, whereas the softness ones are dominated by the elastomeric organic polymer chains. Some plastic sites should also correspond to microcracks of the pore wall, revealing pore sites when lower values of the elastic modulus are measured in relation with the pure silica sites (stiffest). These microcracks in the pore wall can be the responsible of the pop-in and pop-out events, in the loading and unloading branch, respectively. Then, when the indenter travels without a measured increase in load provoke the discontinuities in the depth–load hysteresis curve as can be seen by the arrows pointed out in the inset of Fig. 2, as a general rule these events are related with molecular rearrangements, in that case fractures produced in the pore wall. In order to illustrate such microstructure, Fig. 3 shows a picture of the aerogel PDMS60, in which the porosity is apparent.

The 2D resulting map is depicted in Fig. 4(a) for the reduced elastic modulus, where it is apparent the above mentioned stiff (white) and soft (black) sites. In this way, stiffer sites correspond to the lower elastic recovery and consequently to the maximum plastic depth as a characteristic of the pure silica.

On the other hand, the softer sites correspond to the maximum elastic recovery characteristic of the elastomeric chains behaving as a spring (hookean solid). This result is corroborated in the 2D map of the elastic recovery parameter (Fig. 4(b)), in which elastic sites (white) correspond to the lower reduced modulus and plastic ones (black) correspond to the hard areas of the aerogel.

As a matter of fact, we have take the reduced modulus as Young's modulus (given the big difference in relation to that of the diamond), its evolution as a function of the polymer content has a decreasing trend. Fig. 5 shows such plot of the Young's modulus versus polymer content. The average value (solid star) is included with the error bars. The macroscopic Young's modulus from uniaxial compression (solid rhomb) is also included;

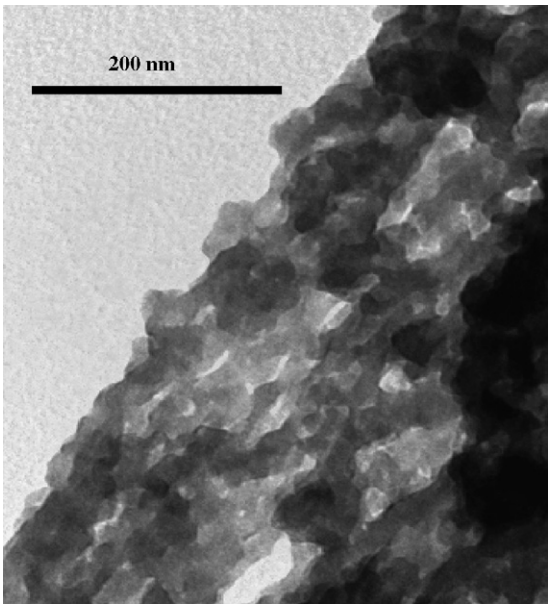

Fig. 3. Transmission electronic micrograph (TEM) of the aerogel sample PDMS60.

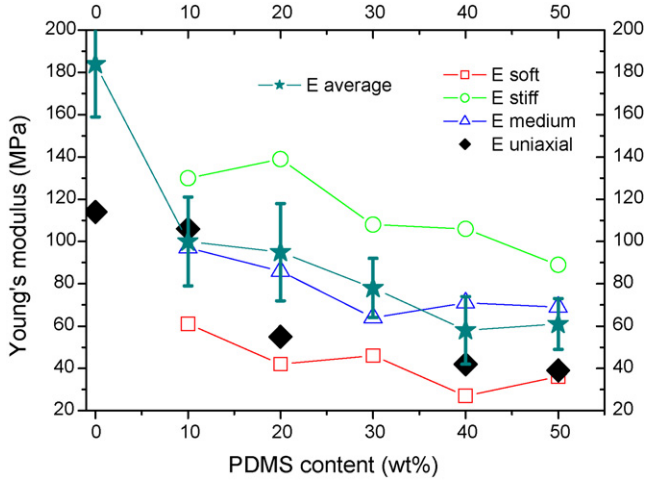

Fig. 5. Elastic modulus as a function of the polymer content.

this value comes closer to that of the softer sites indicating that the polymer phase controls the mechanical behaviour at the macroscopic level. The silica clusters bonded by means elastomeric chains as springs act as a dashpot giving the final elastic modulus of a soft material.

Keeping in mind the above results we have performed several experiments to corroborate it. The experimental creep curves show the typical saturation shape with an instant deformation, and then the primary regime of retarded strain and secondary creep of steady state linear regime. It can be seen that the depth of the retarded strain is much higher in the hybrid aerogel than that in the pure silica one. Some typical creep curves from our samples are shown in Fig. 6. Occasionally at low loads, we found that during the steady state, the competition between strain and recovery mechanisms was won by the recovery ones, yielding to the material to push off the tip. These atypical curves can be seen in the inset of Fig. 6. It can bee seen as well that in the hybrid aerogel at 0.75 mN the recovery and creep processes

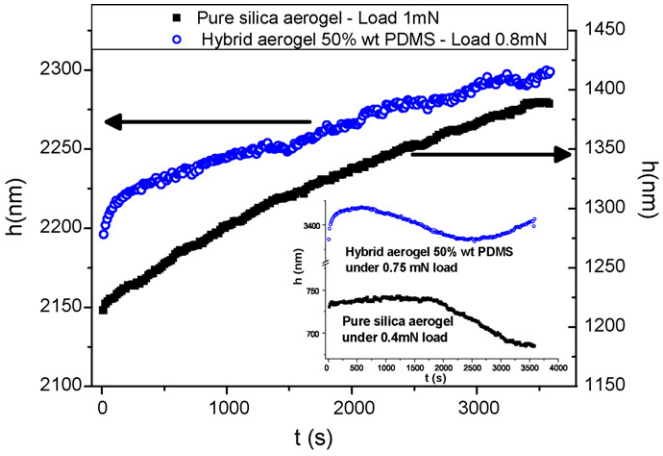

Fig. 6. Two examples of typical creep curves in two different aerogels, at different loads. In the inset, two anomalous creep curves obtained at low loads, where the steady state is lost by starting a recovery process (pure silica aerogel) or even is not achieved due a continuous competition between strain and recovery processes (hybrid aerogel).

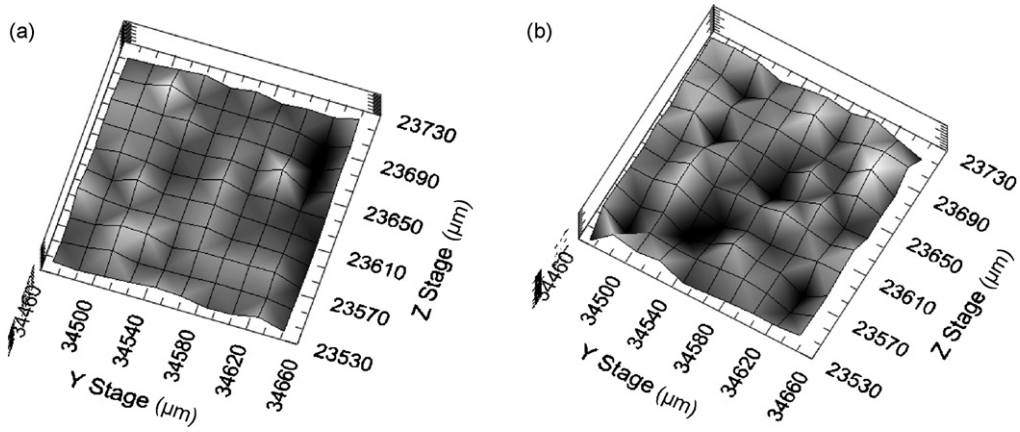

Fig. 4. 10 × 10 grid maps for the PDMS50 sample, for the elastic modulus (a) and for the elastic recovery parameter (b). Each indentation is separated 20 μm.

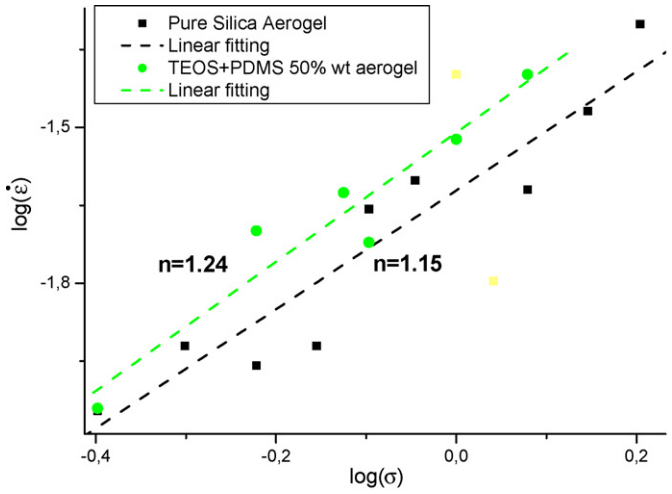

Fig. 7. Log–log strain rate as a function of the applied load, linear fitting and the slope values are included.

are in continuum competition. These results show a particular feature of these materials, that in these conditions it is able to start a recovery process after the instant and retarded strains, in a relative short time. Generally speaking, this time is around half an hour.

For studying the steady state, the log–log strain rate versus applied load has been plotted, as can be seen in Fig. 7. From the slope, is easy to see how these materials are very close to the characteristic value of $n = 1$ expected for amorphous materials. The slope for the pure silica sample is 1.15 and for the composite material increases up to 1.24. Despite the hybrid aerogel is 50 wt.% polymer content, the rheological behaviour is very influenced by the porous silica matrix, as the creep rate keeps close to 1.15.

We obtained also the creep compliance and some of the resulting curves can be seen in Fig. 8. The values of the pure silica and hybrid aerogel differ in more than one order of magnitude, as it was expected due to the presence of the more compliant polymeric phase. If the different regimes of the creep tests are analyzed more deeply, it can be tested the more instantaneous

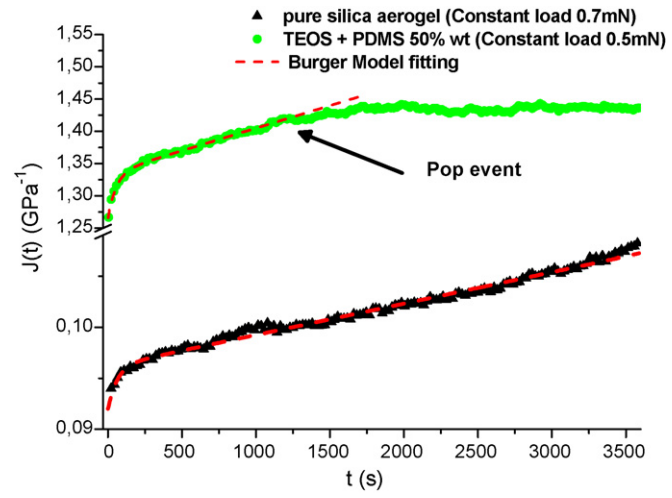

Fig. 8. Creep compliance and Burger model fitting for the outlined samples.

and retarded deformation that shows the hybrid aerogel, as well as the greater slope what indicates lower viscosity on the hybrid one. Some pop-in events suddenly appeared during the creep test changing the response of the material, quitting the steady state and starting a new creep process, as can be seen in the curve of the hybrid aerogel in Fig. 8. The Burger model was used for understanding the rheological behaviour of our materials and the different mechanisms that appears. It was perfectly fitted for different tests at different loads as can be seen in Fig. 8. At a first glance, it can be assumed that the Burger-like behaviour is a very accurate model for these samples. Adding an organic phase to an inorganic pure silica porous matrix yields to reduce significantly the stiffness of the Voigt element, as well as to increase the relaxation time of the transient regime.

As a matter of fact, these aerogels could be good candidates as substitutive of the cancellous human bones.

4. Conclusions

The inclusion of polymeric organic chains in inorganic silica aerogel matrix produces a rubber-like material. Nanoindentation maps reveal the heterogeneities of these solids, stiff zones locating the tough silica matrix, soft zones indicating the areas where the polymer is located and plastic zones produced by the pores. The elastic modulus decreases with the polymer content. The macroscopic elastic modulus matches satisfactorily the values obtained by nanoindentation, so this confirms the validity of nanoindentation as a useful tool for study this kind of materials and therefore allows us to consider the values as a reference not only at a micrometer scale. In our case, the higher the organic content is, the better the correspondence is between macro and microscopic values, what let us to conclude that polymer chains govern the macroscopic response.

Creep tests showed that creep compliance values increased more than one order of magnitude with the addition of the polymer to the aerogel. From the theoretical analysis of the rheological behaviour with the fitting of the Burger model, it can be assumed that the addition of the polymer acts mainly on the transient regime, namely, on the Voigt element of the model. The steady state is also affected, but is controlled by the inorganic phase, as the creep rate is maintained on similar values for both samples.

Acknowledgments

The authors are grateful for the financial support from the Spanish Government: Ministerio de Ciencia y Tecnología (Project MAT2005-1583) and to the Junta de Andalucía (TEP 0115).

References

1. Schuh, C. A., Nanoindentation studies of materials. *Mater. Today*, 2006, **9**, 32–40.
2. Marshall, G. W., Habelitz, S., Gallagher, R., Balooch, M., Balooch, G. and Marshall, S. J., Nanomechanical properties of hydrated carious human dentin. *J. Dent. Res.*, 2000, **80**, 1768.

3. Ebenstein, D. M. and Pruitt, L. A., Nanoindentation of soft hydrated materials for application to vascular tissues. *J. Biomed. Mater. Res. A*, 2004, **69A**, 222.
4. Carrillo, F., Gupta, S., Balooch, M., Marshall, S. J., Marshall, G. W., Pruitt, L. *et al.*, Nanoindentation of polydimethylsiloxane elastomers: effect of crosslinking, work of adhesion, and fluid environment on elastic modulus. *J. Mater. Res.*, 2005, **20**, 2820–2830.
5. Moner-Girona, M., Roig, A., Molins, E., Martínez, E. and Esteve, J., Micromechanical properties of silica aerogels. *Appl. Phys. Lett.*, 1999, **75**, 653–655.
6. Blanco, E., Esquivias, L., Litran, R., Piñero, M., Ramírez-del-Solar, M. and de la Rosa-Fox, N., *Appl. Organomet. Chem.*, 1999, **13**, 399.
7. Piñero, M., Morales-Flórez, V., de la Rosa-Fox, N. and Esquivias, L., Mechanical properties of hybrid aerogels. *Bol. Soc. Esp. Ceram. V*, 2005, **44**(5), 291–293.
8. Ferry, J. D., *Viscoelastic Properties of Polymers* (*3rd ed.*). Wiley, New York, 1980.
9. Callister, Jr., W. D., *Introducción a la Ciencia e Ingeniería de los Materiales*. Reverté, Barcelona, 1995.
10. Zarzycki, J., *Glasses and the Vitreous State*. University Press, Cambridge, 1991.
11. Huber, N. and Tsakmakis, Ch., Discussion of finite deformation viscoelasticity laws with reference to torsion loading. *Continuum Mech. Thermodyn.*, 2000, **12**, 303–323.
12. Möginger, B., The determination of a general time creep compliance relation of linear viscoelastic materials under constant load and its extension to nonlinear viscoelastic behaviour for the Burger model. *Rheol. Acta*, 1993, **32**, 370–379.
13. Sills, S., Fong, H., Buenviaje, C., Sarikaya, M. and Overney, R. M., Thermal transition measurements of polymer thin films by modulated nanoindentation. *J. Appl. Phys.*, 2005, **98**, 014302.
14. Adalja, S. B. and Otaigbe, J. U., Creep and recovery behavior of novel organic–inorganic polymer hybrids. *Polym. Compos.*, 2002, **23**(2), 171–181.
15. Oliver, W. C. and Pharr, G. M., An improved technique for determining hardness and elastic modulus using load and displacement sensing indentation experiments. *J. Mater. Res.*, 1992, **7**, 1564–1583.
16. Pharr, G. M., Oliver, W. C. and Brotzen, F. R., On the generality of the relathionship among contact stiffness, contact area, and elastic modulus during indentation. *J. Mater. Res.*, 1992, **7**, 613–617.
17. Tsou, C., Hsu, C., Fang, W., Lai, T. S. and Li, H.C., Characterization of the bending creep behaviour for electroplating nickel microbeam. In *IEEE 6th International Conference on Electronic Packaging Technology*, 2005, 0-7803-9449-6/05.
18. Li, J. and Dasgupta, A., Failure-mechanism models for creep and creep rupture. *IEEE Trans. Reliab.*, 1993, **42**(3), 339–353.
19. Pérez-Prado, M. T., McNelley, T. R., Swisher, D. L., González-Doncel, G. and Ruano, O. A., Texture analysis of the transition from slip to grain boundary sliding in a continuously recrystallized superplastic aluminum alloy. *Mater. Sci. Eng. A*, 1998, **244**, 216–223.
20. Lu, H., Wang, B. and Viswanathan, H., Measurement of creep compliance of solid polymers by nanoindentation. *Mech. Time-Dep. Mater.*, 2003, **7**, 189–207.
21. VanLandingham, M. R., Sung, L. P., Chang, N. K., Wu, T. Y., Chang, S. H. and Jardret, V. D., Measurement approaches to develop a fundamental understanding of scratch and mar resistance. *JCT Res.*, 2004, **1**(4), 257–266.